JOURNAL OF SOLID STATE CHEMISTRY 84, 23–38 (1990)

High Resolution Electron Microscopy Study in the $NaNbO_3$–Nb_2O_5–WO_3 System

MARGARETA SUNDBERG AND BENGT-OLOV MARINDER

Department of Inorganic Chemistry, Arrhenius Laboratory, University of Stockholm, S-106 91 Stockholm, Sweden

Received June 1, 1989

High resolution electron microscopy studies have been made in the system $NaNbO_3$–Nb_2O_5–WO_3 with emphasis on the following two lines in the phase diagram: $Na_{2-x}M_6O_{16}$, $0 < x < 2$, and $Na_{1.50-x}M_{6.1}O_{16}$, $0 < x < 1.5$, M = Nb, W. The presence of four structure types, three of which are related to the tetragonal tungsten bronze (TTB) type, has been revealed. The X-ray diffraction patterns only indicated a basic TTB structure in this region. The fourth one, observed in a sample of composition $Na_{1.40}Nb_{6.12}O_{16}$, is isotypic with $NaNb_6O_{15}F$. The most frequently observed TTB structure is of the $Nb_8W_9O_{47}$ type, consisting of three basic TTB unit cells with four pentagonal columns (PCs) in the triple unit. The second most common phase type is $NaNb_5WO_{16}$ isotypic with $KNb_{12}O_{29}F_3$ (with a structure comprising two basic TTB unit cells, with four PCs in a square arrangement) which has a doubled content of alkali atoms. A third TTB-related structure observed in $Na_{1.41}Nb_{6.01}W_{0.09}O_{16}$ is isotypic with $KNb_6O_{15}F$ (with two basic TTB unit cells and with two PCs connected by a common octahedron). There are indications that an excess of transition metal stabilizes this phase as well as the $NaNb_6O_{15}F$ type phase. Twinning, defects, and intergrowth of TTB-related phases are frequently observed phenomena.

Introduction

A couple of years ago Marinder (*1*) reviewed the phases in the $NaNbO_3$–Nb_2O_5–WO_3 system. The discussion was focused on phases found by X-ray and thermal analysis methods. Only a few results obtained by electron microscopy were included. Some structures were reported to be related to the tetragonal tungsten bronze structure.

In the top part of Fig. 1a the skeleton structure of TTB and its unit cell are shown. The structure is built up of corner-sharing MO_6-octahedra arranged so that three-, four-, and five-sided tunnels are formed, where the sodium atoms are located in the last two types of tunnels (*2*, *3*). The unit cell content of TTB can be expressed by the formula $A_xM_{10}O_{30}$, where A is a tunnel atom and $x \leq 6$.

Superstructures with oxygen-to-metal ratios of less than 3 are formed when strings of alternating metal (M) and oxygen atoms, $-M-O-M-O-$, enter the five-sided tunnels. The structural building unit so formed, a pentagonal bipyramid sharing edges with five corner-sharing MO_6-octahedra, is called a pentagonal column (PC) (*4*). A symbolism (Fig. 1b) for the visualization of PCs has been given (*5*). The first superstructure of TTB type was reported for the $Nb_8W_9O_{47}$ compound (*6*). The lower parts of Figs. 1a and b illustrate that this struc-

0022-4596/90 $3.00

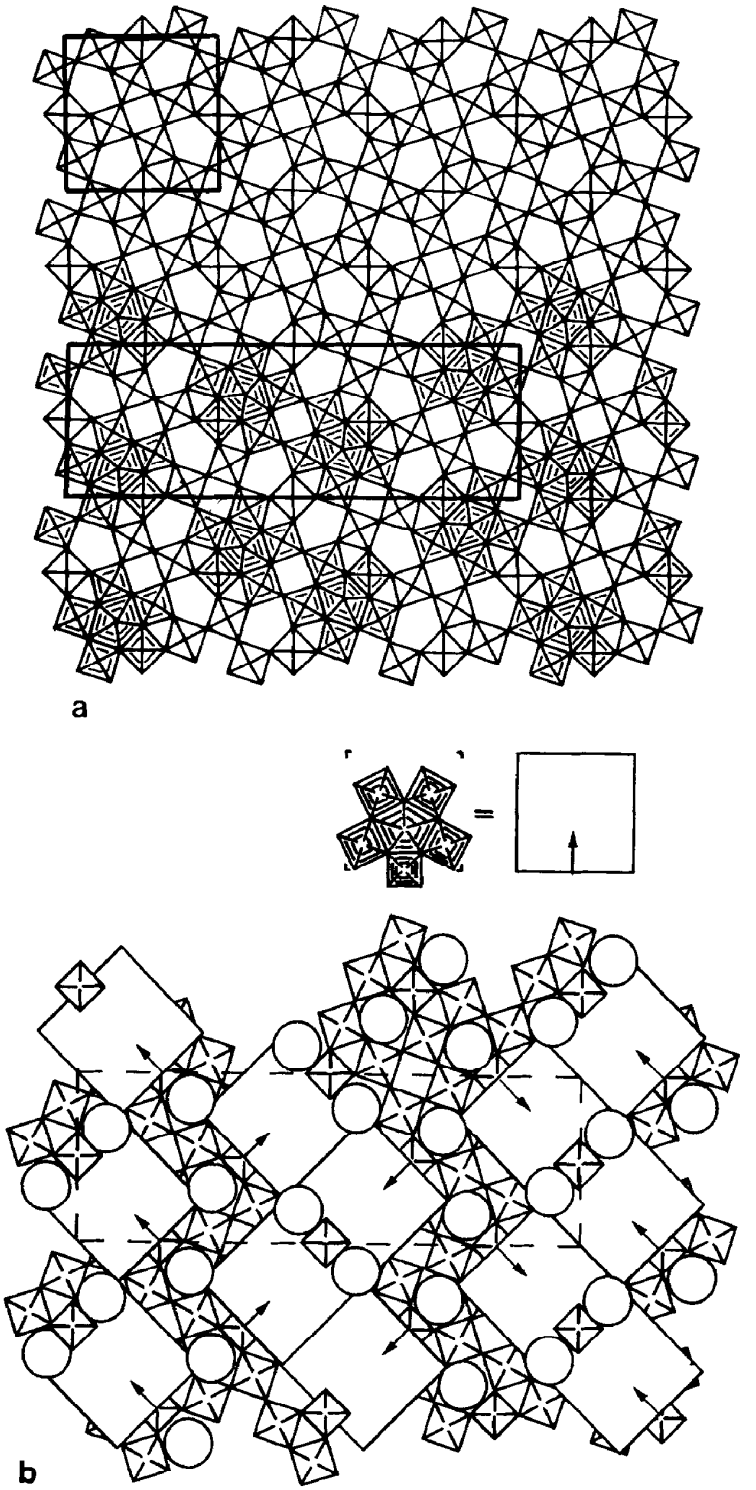

FIG. 1. (a) The basic TTB framework structure is shown at the top and the $Nb_8W_9O_{47}$ (D-3TTB) type structure in the lower part of the figure. The corresponding unit cells are drawn. (b) An alternative way of illustrating the D-3TTB structure in (a). Circles indicate five-sided tunnels. A pentagonal column (PC) and its symbol are shown at the top.

ture has a unit cell three times the size of the TTB cell with orthorhombic symmetry. Four out of twelve five-sided tunnels have been transformed to PCs in such a way that an ordered arrangement of diamond-linked pairs (see below) of PCs is formed. The composition of the unit cell can thus be written as $(MO)_4M_{30}O_{90}$ (M = Nb, W). In the following this superstructure will be denoted D-3TTB, where D and 3 indicate the occurrence of *diamond*-linked pairs of PCs in a unit cell composed of 3 TTB cells. A system of notation of TTB-related structure types has been given in (*7*). The phase diagram in Fig. 2 illustrates that TTB- and D-3TTB-related phases are formed within an extended region from $Nb_8W_9O_{47}$ down to the $NaNb_3O_8$ phase (*8*).

In a recent study of phases in the $KNbO_3$–Nb_2O_5–NbO_2F system (*9*), seven different TTB-related phases have been discovered by a combination of high resolution electron microscopy (HREM) and X-ray powder diffraction methods. The region of existence of each structure type was given, and various types of twinning, defects, and intergrowths between the observed phases were reported.

As a result of the review of the title system it became apparent to us that we had to complement the X-ray diffraction methods by HREM in order to elucidate the structural details encountered. This was the case in the structure determination of $Na_7Nb_{15}W_{13}O_{80}$ (*10*), and very much so as regards our structural studies of $NaNb_7O_{18}$ (*11*). Further studies of samples in the $NaNbO_3$–Nb_2O_5–WO_3 system have shown that they differ to some extent from those of the $KNbO_3$–Nb_2O_5–NbO_2F system (*9*) concerning the type of TTB-related phases formed and their regions of existence. Some of these results will be presented below.

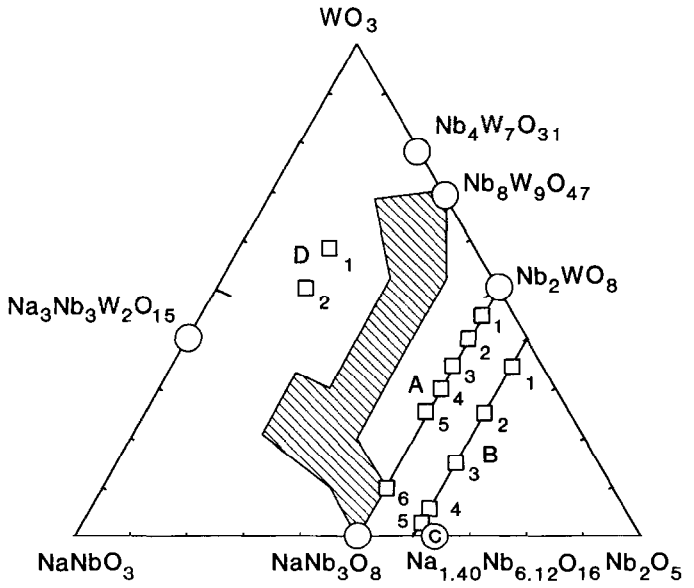

FIG. 2. TTB-related phases in the system $NaNbO_3$–WO_3–Nb_2O_5. Also indicated are Nb_2WO_8 (of $LiNb_6O_{15}F$ type), $Na_{1.40}Nb_{6.12}O_{16}$ (of $NaNb_6O_{15}F$ type), and $Na_{8-x}Nb_{16-x}W_{12+x}O_{80}$ with x = 1 and 2 and with an O/(Nb, W) ratio of 2.857 (D1 and D2). Samples on line A have an O/(Nb, W) ratio of 2.667. Those marked B have a 2.625 ratio. Samples on lines A and B and sample C are discussed in the text. Striation indicates an extended region where TTB-related phases have previously been found (*8*).

Experimental

Samples were prepared by heating finely ground mixtures of $NaNbO_3$ (Pierce Inorganics B.V.), Nb_2O_5 (Merck, optipure, heated for several hours at 1370 K in air), and WO_3 (B.D.H., Laboratory Reagent) at 970 K for 1 day and at 1070 K for 4 or 5 days in sealed platinum tubes. At the end of the heating period we rapidly cooled the tubes to room temperature by simply removing them from the furnace. The samples, which were colorless and microcrystalline, were reground, heated for the same period of time, and cooled. They were examined in a Guinier–Hägg focusing camera. The technique used and the evaluation of the results are described in Ref. (*8*).

Specimens for HREM were prepared by crushing a small amount of the sample in an agate mortar. The powder was then suspended in *n*-butanol and a drop of the suspension deposited on a holey carbon film supported on a Cu-grid. The grids were studied in a JEOL 200CX electron microscope, equipped with a high resolution top-entry goniometer stage with tilt angles of $\pm 10°$. The accelerating voltage used was 200 kV. Electron diffraction patterns were recorded of thin crystal fragments oriented so that either the [100] or [001] zone axis was parallel to the electron beam. HREM images were taken of flakes aligned with the short crystal *c*-axis (~3.9 Å) parallel to the beam. An objective aperture corresponding to a radius of 0.41 $Å^{-1}$ in the diffraction pattern was used. Simulations of HREM images were made by using the SHRLI set of programs (*12*) based on the multislice method.

Results

A. The Line $Na_{2-x}Nb_{6-x}W_xO_{16}$ ($0 < x < 2$)

The X-ray diffraction patterns of samples of gross compositions along this line (see Fig. 2) indicated the presence of a phase related to the TTB type. Single-phase samples could not be obtained, however; a few weak reflections from H–Nb_2O_5 were always present.

Electron diffraction patterns from fragments of samples in the region $1.8 \geqq x \geqq 1.2$ (A1–A4 in Fig. 2) were all similar and showed that the substructure was of TTB type ($a_{TTB} \sim 12.5$ Å). The typical pattern illustrated in Fig. 3 shows that superstructure reflection spots are present, indicating a tripling of one of the a_{TTB}-axes; frequent twinning of this superstructure is observed. Figure 3 also shows that weak diffuse scattering appears as almost circular rings around the subcell reflections. These circles are to some extent caused by streaking of the superstructure spots, and they indicate some amount of disorder in the structure.

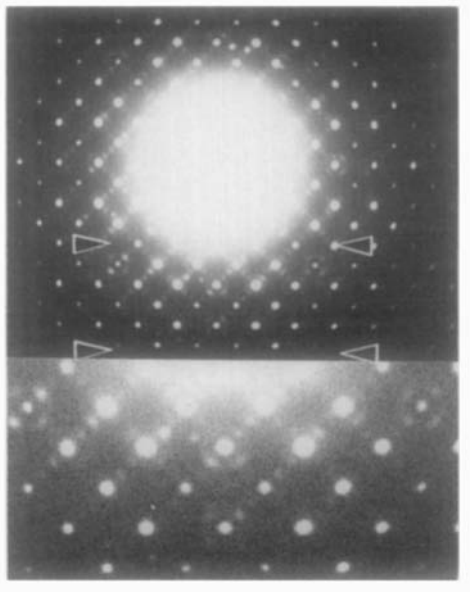

FIG. 3. The electron diffraction pattern of a thin fragment from the $Na_{0.20}Nb_{4.2}W_{1.8}O_{16}$ sample (see A1 in Fig. 2) shows weaker superstructure spots indicating a tripled TTB unit cell. There is also twinning and circular diffuse scattering. The latter two phenomena indicate a very disordered crystal fragment. The region within the arrows is enlarged and shown at the bottom of the figure.

From electron diffraction patterns of thin crystal fragments projected along [100], it was obvious that the short c-axis was doubled, as weak diffuse layer lines with only a few superstructure reflections appeared between the strong distinct layer lines. The doubling of the short c-axis is probably caused by a slight displacement of the metal atoms from the center of the MO_6-octahedra, as observed in several other transition metal oxides.

The low magnification micrograph in Fig. 4a illustrates that the corresponding crystal fragment is heavily disordered and largely built up of microdomains with a lattice of dimensions $a_0 = a_{TTB}$, $b_0 = 3 \times a_{TTB}$. The domains are either mutually displaced by $\frac{1}{3}b_0$ (see arrows in Fig. 4a) or appear in twin orientation. The contrast features and the size of the unit cell as well as the appearance of the electron diffraction pattern indicate that the microregions can be interpreted as being built up mainly of a D-3TTB type structure. However, from the recorded micrographs the concentration of PCs seems to be somewhat higher at the boundaries than that in the ordered domains. An enlargement of a part of the thin crystal edge in Fig. 4a is shown in Fig. 4b, with an interpretation of the area enclosed in the box given in Fig. 4c. The interpreted region is composed of 17 TTB unit cells, where 27 out of 68 five-sided tunnels have been transformed to PCs. This corresponds to a local filling of 39.7%, which is somewhat higher than 33.3% for the D-3TTB type structure. Figure 4d shows the PCs of Fig. 4c in an alternative way (cf. Fig. 1b).

The electron diffraction study of the $NaNb_5WO_{16}$ sample (x = I, A5 in Fig. 2) showed three different patterns, all of which indicated TTB-related phases. The first type contained the same features as shown in Fig. 3. The corresponding HREM image also revealed a disordered and twinned structure of D-3TTB structure type, similar to that reported above (Fig. 4a).

The second type of pattern could be interpreted as yielding from a TTB-related phase with a unit cell of $a \sim a_{TTB}\sqrt{2}$. The contrast features in the corresponding HREM image in Fig. 5a demonstrate that this phase is isostructural with $KNb_{12}O_{29}F_3$ (*7*) and $Na_3Nb_{12}O_{31}F$ (*13*). The structure model is shown in Fig. 5b and in an alternative way in Fig. 5c. The composition of this model can be written as $A_y(MO)_4M_{20}O_{60}$, where y is equal to the number of tunnel atoms (A). Four out of eight five-sided tunnels have been filled with $-M-O-M-O-$ strings and transformed to PCs, and this is thus a case of 50% filling of the five-sided tunnels. In this structure there is an ordered arrangement of squares of four PCs, separated by squares of four five-sided tunnels where the A atoms reside. This superstructure of TTB type has previously been denoted S-2TTB (*7*), where S stands for a *square* of PCs and 2 indicates a unit cell volume *twice* that of TTB.

If we assume the composition $NaNb_5WO_{16}$ for this type of crystal, we have to insert four sodium atoms into the model to obtain agreement between composition of the prepared material and the model shown. The sodium atoms can enter both four- and five-sided tunnels. Simulation of HREM images have been performed, starting from the model in Fig. 5b with four sodium atoms located in the four five-sided tunnels. The atomic coordinates given for Nb and O in the single-crystal X-ray study of $Na_3Nb_{12}O_{31}F$ (*13*) were used in these calculations. There is good agreement between the experimental image in Fig. 5a and the calculated image in Fig. 5d.

In agreement with previous results obtained in the KNb_3O_8–Nb_3O_7F system (*7*), the calculations of HREM images for different crystal thicknesses and defocus values showed that it is not possible to determine the position and occupancy of Na atom sites in the tunnels. In spite of full occupancy of the Na sites in the five-sided tunnels, all tunnels appear with almost the

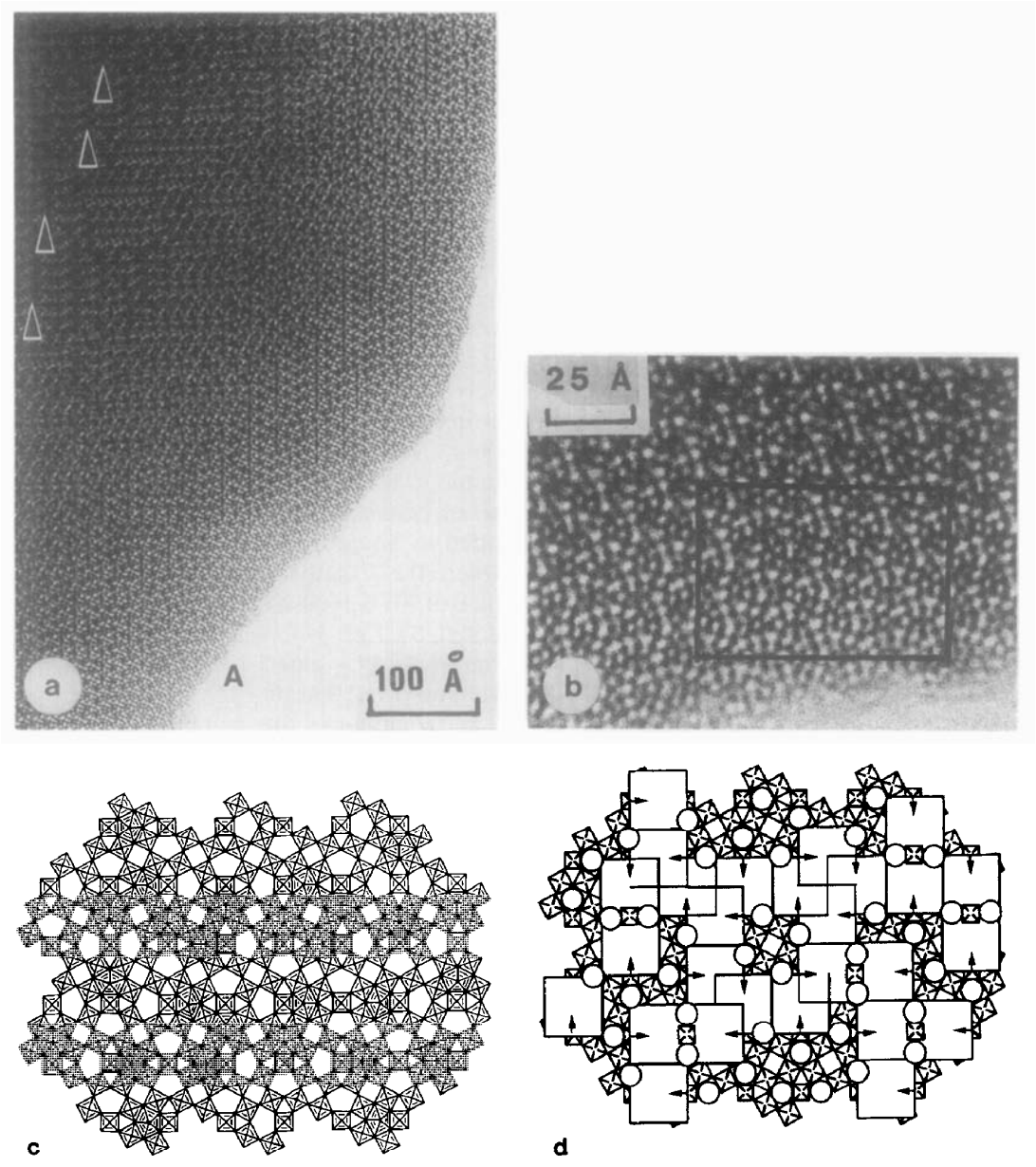

FIG. 4. (a) Low magnification image of a thin fragment from the $Na_{0.40}Nb_{4.4}W_{1.6}O_{16}$ sample projected along [001]. The mutual displacement of two D-3TTB microdomains by $\frac{1}{3}b_0$ at the boundary is indicated by arrows. (b) Enlargement of the thin crystal edge at A. (c) Structure model showing the interpretation of the region enclosed in the box in (b). (d) The same model as that in (c) but with PC symbols.

same, white, contrast except at Scherzer focus (−600 Å), where a very faint contrast due to the Na atoms can be discerned. However, this defocus value cannot be used to determine the type of TTB-related structure with certainty. The HREM images have to be recorded at a defocus value of (~−400 Å) where the contrast in the im-

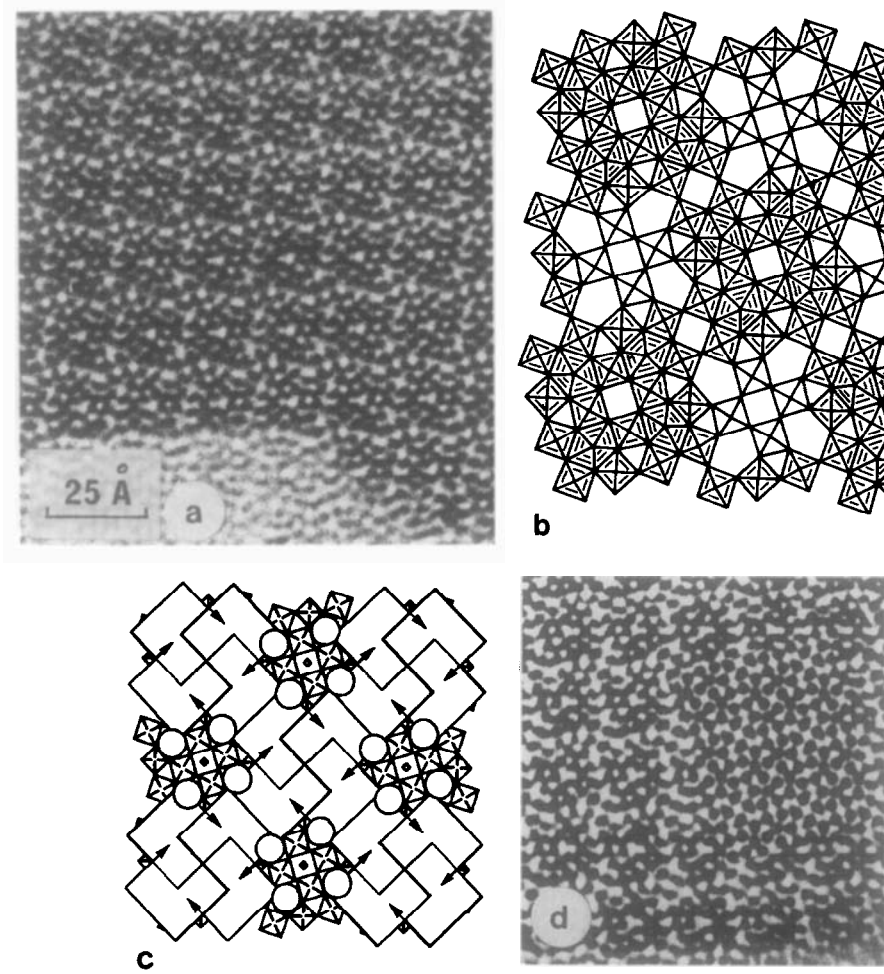

FIG. 5. (a) HREM image of a thin fragment from the $NaNb_5WO_{16}$ sample (A5 in Fig. 2). (b) The structure model of $NaNb_5WO_{16}$ (S-2TTB) isotypic with $KNb_{17}O_{29}F_3$ (7). The sodium atoms in the tunnels are not shown. (c) The same model as that in (b) but with PC symbols. (d) Part of the HREM image in (a) with a simulated image of the structure model in (b) inserted to the right. Crystal thickness ~20 Å. Defocus value −440 Å.

ages is high, and distinct white tunnels appear. At this defocus value the PC arrangement and hence the type of TTB structure can be determined with certainty. Intergrowth of various TTB type structures can also be revealed under these conditions.

The third type of pattern, from fragments of the $NaNb_5WO_{16}$ sample, could be interpreted as a superposition of the first two types of diffraction patterns, which means that an intergrowth of D-3TTB and S-2TTB should be observed in the corresponding HREM images. The example shown in Fig. 6 illustrates that the examined fragment is composed of domains of S-2TTB structure type intergrown with domains of D-3TTB phase.

The results obtained from the $Na_{1.60}Nb_{5.6}W_{0.4}O_{16}$ sample ($x = 0.40$) (A6 in Fig. 2) were similar to those reported above for

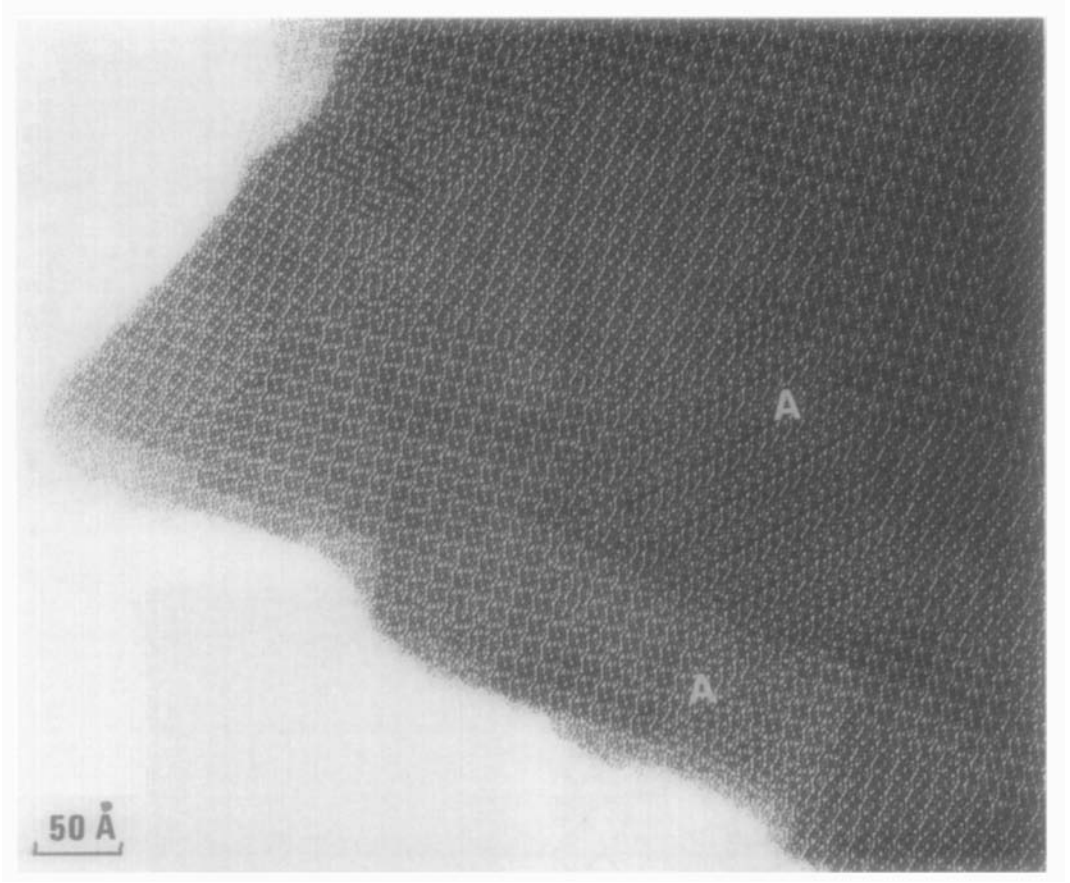

FIG. 6. Low magnification micrograph showing domains of S-2TTB type structure intergrown with domains of D-3TTB type structure (marked A).

specimens in the region $1.8 \geq x \geq 1.2$, as the electron diffraction patterns indicated a twinned D-3TTB type structure with some very weak traces of diffuse circles around the TTB subcell reflections. The low magnification image in Fig. 7a also reveals a twinned structure similar to that of D-3TTB type, with some disorder at the twin boundaries. The domains seem to be slightly larger than those reported above. Figure 7b shows an enlargement of a part of the edge in Fig. 7a, and an interpretation of the area marked is given in Figs. 7c and 7d. At some places marked by arrows in Figs. 7a, 7b, and 7c, the contrast features in the image can be interpreted as a row where PCs are mutually linked by a common MO_6-octahedron. Figures 7c and 7d demonstrate that the interpreted region is built up of a D-3TTB structure "diluted" by these pairs of mutually linked PCs (see arrows in Figs. 7a, 7b, and 7c), and hence a defect D-3TTB type structure is formed. Alternatively, the structure in Fig. 7c can be considered as thin slices of M-2TTB structure intergrown into the D-3TTB phase. The region in Fig. 7c is composed of 3 × 6 TTB unit cells, where 30 out of 72 five-sided tunnels have been filled with –*M*–O–*M*–O– strings, giving a local filling of 41.7%, which is higher than the 33.3% filling in the D-3TTB structure. Figure 7a also illustrates that microre-

gions composed of only a few unit cells of the S-2TTB type structure coexist with large regions of the defect D-3TTB phase. An example is marked by A in Figs. 7a and 7b. Figure 7b also shows that the domain boundary at A is built up of TTB unit cells where three out of four five-sided tunnels have been transformed to PCs, hence, giving a local composition between the D-3TTB and the S-2TTB phase compositions.

B. The Line $Na_{1.50-x}Nb_{6.10-x}W_xO_{16}$ $(0 < x < 1.5)$

According to the Guinier powder patterns, these samples appeared to contain two phases; one was TTB related and the other was H–Nb_2O_5 (always in small amounts).

Electron microscopy studies of these samples revealed that D-3TTB was the most frequently occurring structure type. It was found at least in some fragments of all samples examined. For large x-values (x = 1.31 and x = 0.93, B1 and B2 in Fig. 2) the recorded electron diffraction patterns frequently showed diffuse circles around the TTB subcell spots, with only very faint indications of a tripled unit cell, indicative of a D-3TTB type structure with severe disorder. This was confirmed by the corresponding HREM images, which revealed very disordered fragments with microregions of D-3TTB type structure in twin orientations. Single units of four PCs in a square arrangement, as in the S-2TTB phase, could often be discerned in the images. The examined samples seemed to be more disordered and contained a somewhat higher density of PCs than the nearby samples x = 1.80 and x = 1.60 on the $NaNb_3O_8$–Nb_2WO_8 join (A1 and A2 in Fig. 2). This was also confirmed by the electron diffraction study.

The micrograph in Fig. 8, of a crystal fragment from a sample with x = 0.55 (B3 in Fig. 2), illustrates intergrowth of domains of the D-3TTB and $NaNb_5WO_{16}$ (S-2TTB) structure types. The presence of these phases was also confirmed by the electron diffraction pattern. A difference in composition between the D-3TTB and the S-2TTB regions is likely.

Samples with x = 0.17 and x = 0.09 (B4 and B5 in Fig. 2) were found to be multiphase specimens. The main part of the samples consisted of TTB-related phases. A few fragments of H–Nb_2O_5 and a small amount of a phase isotypic with $NaNb_6O_{15}F$ (*14*) could also be identified by electron microscopy. In the x = 0.17 sample only a relatively well-ordered D-3TTB type structure was observed. On the other hand, electron diffraction patterns of some fragments in the x = 0.09 specimen showed TTB subcell reflections with weak streaking along the a_{TTB}-axis. The corresponding micrograph in Fig. 9a reveals a disordered fragment. The contrast in this image indicates a structure isotypic with that previously reported for $KNb_6O_{15}F$ (*7*). This structure, shown in Figs. 9b and 9c, has been denoted M-2TTB type, where M stands for *mutual*, indicating that two PCs have one octahedron in common; 2 denotes a unit cell volume *twice* that of TTB. The ideal composition of the M-2TTB structure in Fig. 9b can be expressed by the formula $A_x(MO)_4$ $M_{20}O_{60}$, where four out of eight five-sided tunnels in the TTB skeleton structure (Fig. 1a, top) are transformed to PCs; hence, a 50% filling of the five-sided tunnels has been achieved. There remain four five-sided and four four-sided tunnels in the structure which can accommodate the sodium atoms. The enlarged micrograph in Fig. 9d demonstrates that the examined fragment is composed of the M-2TTB type structure in domains of different size in twin orientations. An interpretation of a twin region is shown in Figs. 9e and 9f. At A in Fig. 9a, a small region of the previously described S-2TTB phase above can be discerned.

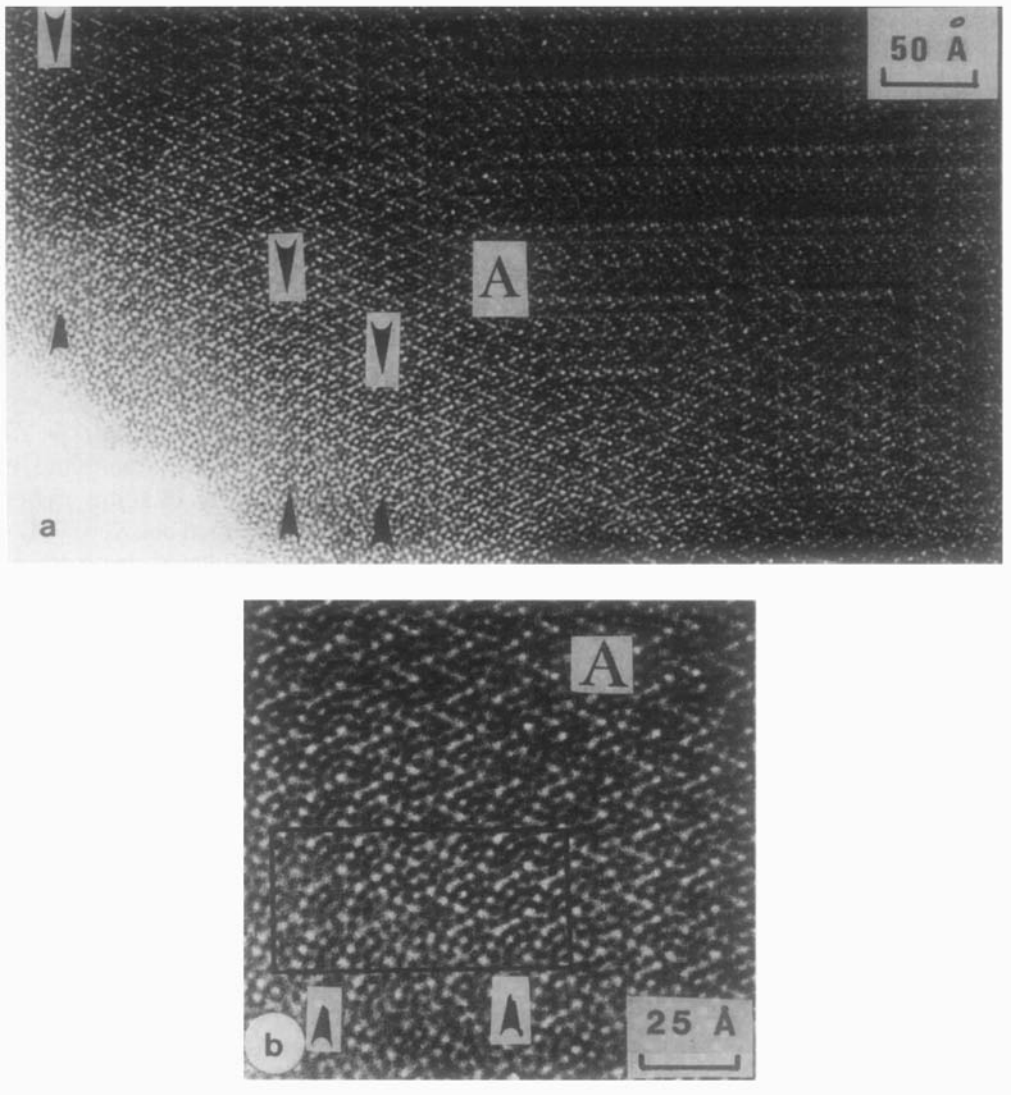

FIG. 7. (a) Low magnification micrograph of a thin crystal fragment from the $Na_{1.60}Nb_{5.6}W_{0.4}O_{16}$ sample (see A6 in Fig. 2). Arrows show rows of PCs mutually linked by a common MO_6-octahedron. (b) Enlargement of a part of the crystal edge in (a). A microregion of the $NaNb_5WO_{16}$ (S-2TTB) phase is marked A. (c) Interpretation of the area enclosed in the box in (b). (d) The same model as that in (c) but with PC symbols.

C. The phase $Na_{1.40}Nb_{6.12}O_{16}$

This compound was first identified as $Na_2Nb_8O_{21}$ ($Na_{1.52}Nb_{6.09}O_{16}$) (*15*). It is stable below 880°C. Its unit cell dimensions and density are given in (*1*); they were based on a sample of composition $NaNbO_3 : Nb_2O_5 = 0.350 : 0.650$. Later experiments with powder diffraction analysis indicate that a composition 0.372 : 0.628 is more probable. This composition, together with the observed density, corresponds to a cell content of $2Na_{1.40}Nb_{6.12}O_{16}$. Its structure is isotypic

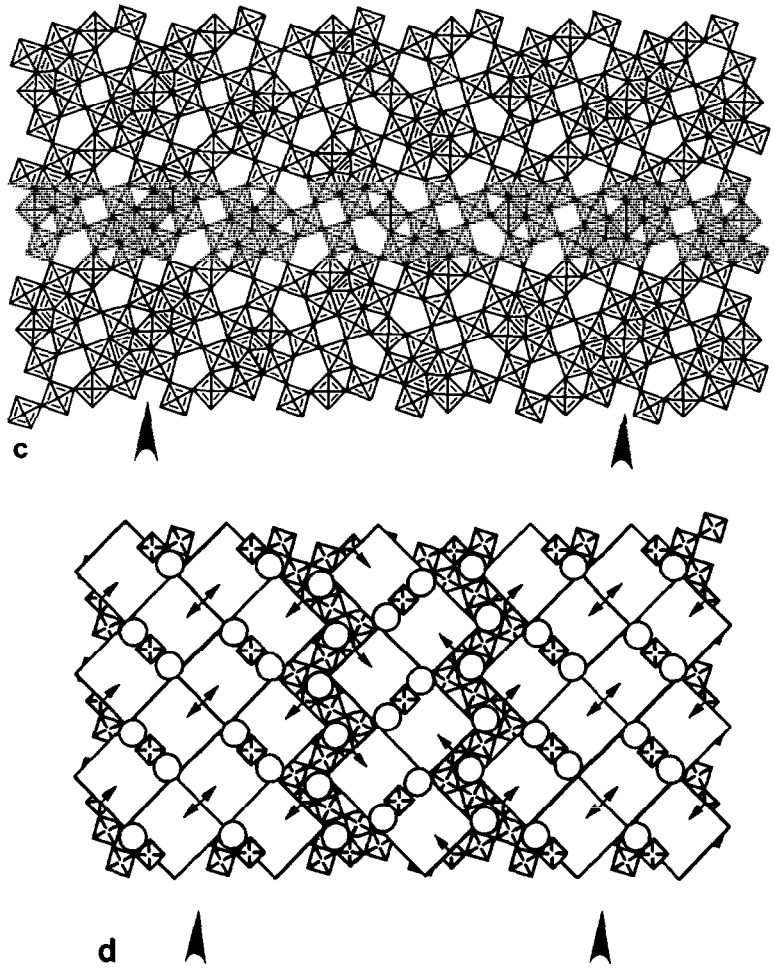

FIG. 7—*Continued*

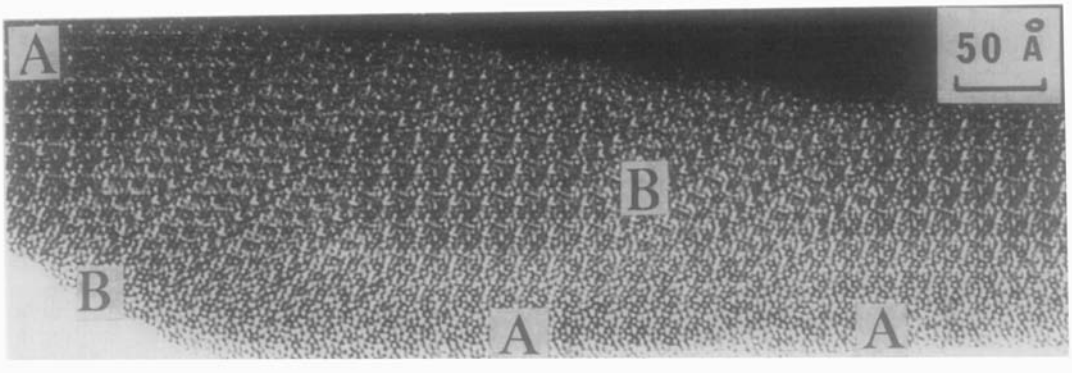

FIG. 8. HREM image illustrating intergrowth of the S-2TTB and D-3TTB phases, marked A and B, respectively.

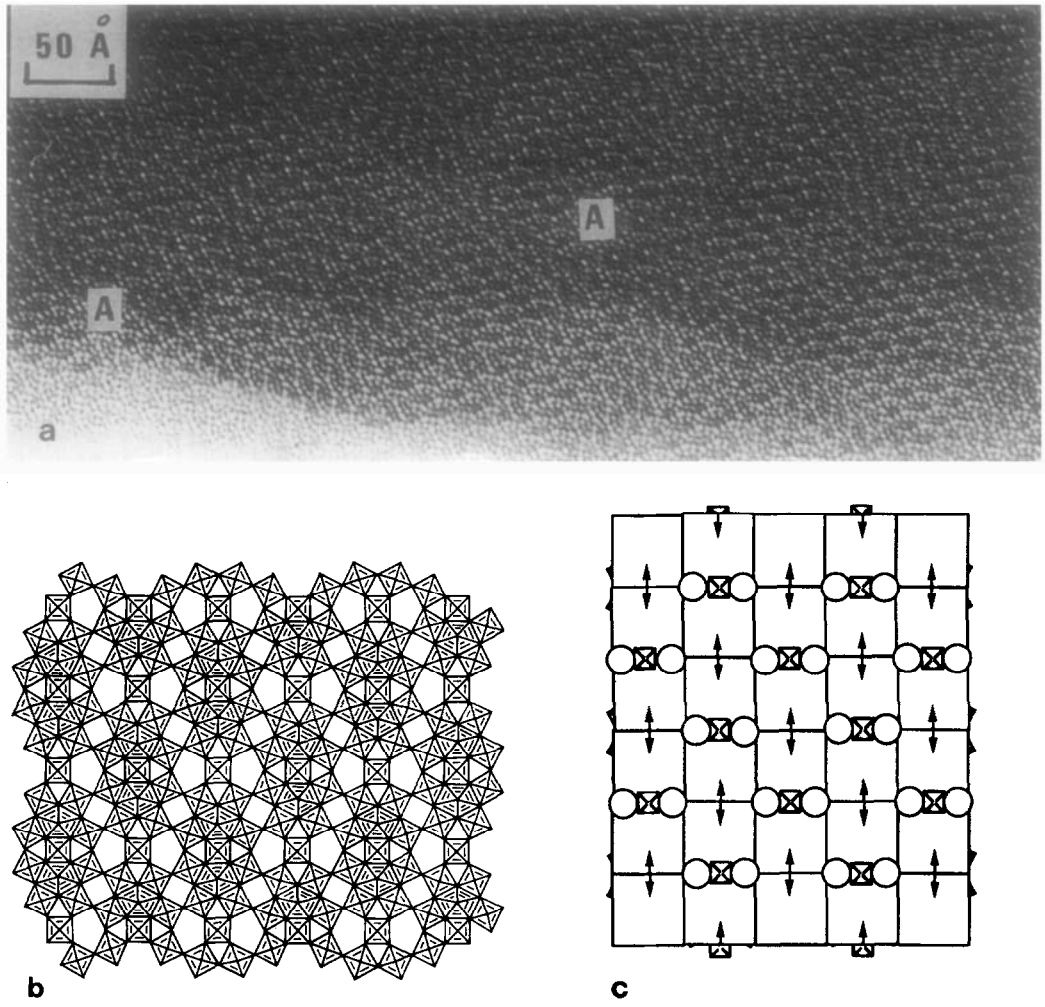

FIG. 9. (a) Low magnification micrograph of a fragment from the $Na_{1.41}Nb_{6.01}W_{0.09}O_{16}$ sample (B5 in Fig. 2) showing domains of M-2TTB type structure in twin orientations. Small areas of S-2TTB type structure (marked A) can also be discerned. (b) Crystal structure model of the M-2TTB phase. The sodium atoms are not shown. (c) The same model as that in (b) but with PC symbols. (d) Enlargement of a part of the crystal edge in (a). (e) Interpretation of the area enclosed in the box in (d). (f) Same model as that in (e) but with PC symbols.

with $NaNb_6O_{15}F$ (*14*). It thus seems that the anion-to-cation ratio in the oxide is much lower than that in $NaNb_6O_{15}F$. If we assume a fully occupied oxygen network, the question of where the extra, "squatter" atoms reside then arises. It is very likely that they settle in some of the trigonal prismatic holes and/or in the diamond-like holes available in the structure (Fig. 10a).

The HREM study showed that twinning was frequent. The HREM image shown in Fig. 10b confirmed the $NaNb_6O_{15}F$ type structure. However, no defects were observed which could explain the discrepancy

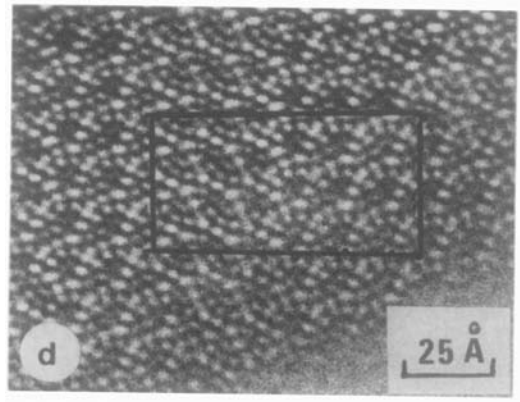

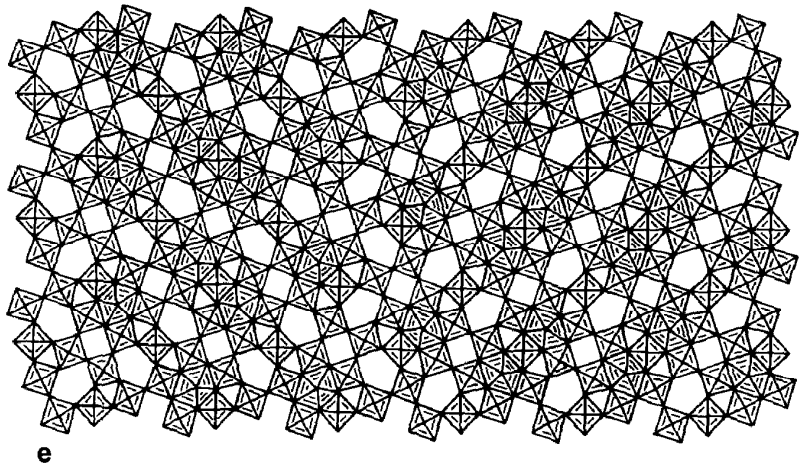

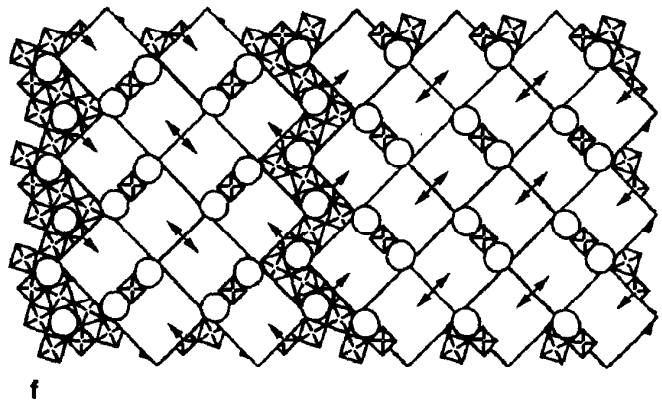

FIG. 9—*Continued*

in composition between the prepared sample and the structure model. Simulated image calculations have previously shown that it is not possible to decide from HREM images whether small amounts of niobium have entered the trigonal holes. The calculated image is inserted into the lower part of Fig. 10b. There is good agreement between

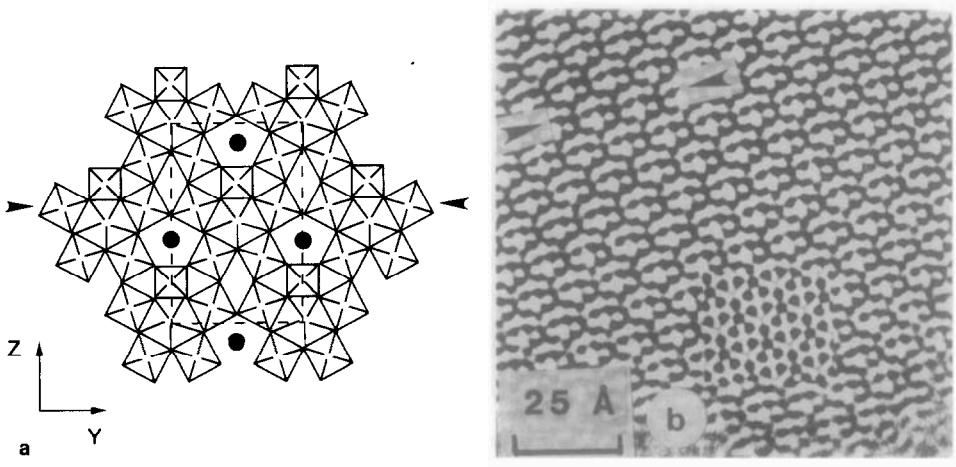

FIG. 10. (a) The crystal structure of $NaNb_6O_{15}F$. The sodium atoms are shown by filled circles. Arrows indicate a row of three PCs joined by corner-sharing. (b) HREM image of a thin crystal fragment from the $Na_{1.40}Nb_{6.12}O_{16}$ sample. Calculated image of the structure model in (a) inserted in the lower part of the HREM image. Crystal thickness ~20 Å. Defocus value −500 Å. Arrows indicate a row of three PCs corresponding to the one shown in (a).

the HREM image and the calculated structure with the assumed composition "$NaNb_6O_{16}$."

Discussion

The electron microscopy results reported above clearly reveal that three different types of TTB-related phases exist in the examined region of the phase diagram, namely, D-3TTB, S-2TTB, and M-2TTB. However, direct agreement between assumed compositions of the examined crystals and the structure models has been obtained only for the S-2TTB phase. In both S-2TTB (Fig. 5b) and M-2TTB (Fig. 9b) type structures 50% of the available five-sided tunnels have been changed to PCs, although the arrangements of the PCs in these structures are quite different. In the $KNbO_3$–Nb_2O_5–NbO_2F system both these types of structures occur on the join KNb_3O_8–Nb_3O_7F, M-2TTB for $KNb_6O_{15}F$ and S-2TTB for $KNb_{12}O_{29}F_3$ (*9*). This means that the alkali content of M-TTB is twice that of the S-2TTB phase. In the $NaNbO_3$–Nb_2O_5–WO_3 system, on the other hand, only the S-2TTB phase is formed on the corresponding join, $NaNb_3O_8$–Nb_2WO_8, but at an alkali composition $NaNb_5WO_{16}$ equal to that of the $KNb_6O_{15}F$ phase (of M-2TTB type).

The Nb_2WO_8–$NaNb_3O_8$ join (line A of Fig. 2) represents an O/*M* ratio of 2.667. This condition is fulfilled for an M-2TTB or an S-2TTB structure type, as can be deduced from their unit cell contents which are given by $A_x(MO)_4M_{20}O_{60}$. In both these structures, four out of eight five-sided tunnels of the TTB skeleton structure have been filled with –*M*–O–*M*–O– strings.

For a sample with an ordinary D-3TTB structure, the O/*M* ratio is 2.765 according to the formula $A_y(MO)_4M_{30}O_{90}$. Here, 4 out of 12 five-sided tunnels are filled with –*M*–O–*M*–O– strings.

A sample with an O/*M* ratio of 2.667 exhibiting a D-3TTB structure would then have the structural formula $A_zM_{1.25}(MO)_4M_{30}O_{90}$ if we assume a fully occupied oxygen network in the structure.

Now the samples on this join were not pure phases, as very faint lines of H–Nb_2O_5 could be discerned on the Guinier photographs. We feel, however, that we cannot disregard the possibility that some small amount of Nb and/or W has entered into the three-sided tunnels in the structure, where nine oxygens may coordinate a metal atom in the center of a tricapped trigonal prism. This is the case in $K_6Ta_{10.8}O_{30}$ (*16*), and similar examples in TTB-related phases may be found in the systems $Pb_{1.36}Nb_{10.91}(O,F)_{30}$ (*17*) and $K_{5.75}Nb_{10.85}O_{30}$ (*18*), and have been disclosed by earlier studies of the present system (*8*).

The composition of the sample with $x = 0.09$ (B5 in Fig. 2) can be given as $Na_{1.41}(MO)M_{5.10}O_{15}$ or $Na_{5.64}(MO)_4M_{20.4}O_{60}$, where M = Nb and/or W. This formula shows that 5.64Na atoms have to be located in the eight available tunnels and that there is a small excess of M atoms, $\sim 0.4M$ per unit cell compared to the M-2TTB structure. The fact that an M-2TTB phase was not found on the A line in the phase diagram, where the composition exactly matches that of the M-2TTB structure, but was observed for a higher Nb_2O_5 content may indicate that excess niobium is essential for the stability of this phase. The small amount of H–Nb_2O_5 observed in the samples makes it likely that the excess is rather small, however. It is also interesting to note that, in comparison with the system KNb_3O_8–Nb_3O_7F, a larger sodium content is necessary for an M-2TTB phase to appear (cf. $\sim Na_{1.41}M_{6.10}O_{16}$ (M = Nb, W) and KNb_6X_{16} (X = O, F)).

Diffraction patterns with circular diffuse scattering around the TTB subcell reflections have previously been reported for the ternary Nb–W–oxide crystals (*19, 20*). De Ridder *et al.* (*19*) have developed a cluster theory to explain the diffuse scattering which, according to these authors, arises from a "transition" state between short and long range order in the structure. This model was applied to the study of order of filling of the five-sided tunnels with –*M*–O–*M*–O– strings in the basic TTB lattice. Agreement was obtained between an experimental HREM image of a crystal with the nominal composition $17Nb_2O_5 \cdot 48WO_3$ (*21*) and the cluster model used. Later, in a study of circular diffuse scattering from a niobium tungsten oxide, $3Nb_2O_5 \cdot 8WO_3$, Horiuchi *et al.* (*20*) explained the observations made by using a slight modification of the cluster model proposed by De Ridder *et al.* (*19*).

The results presented above are in agreement with theoretical calculations on the cluster models. Crystal fragments which gave diffraction patterns with marked diffuse rings were ordered only over microregions, implying that short range order is the predominant ordering in these fragments.

Acknowledgments

The authors thank Professor Lars Kihlborg for valuable comments on the manuscript and Mrs. Gunvor Winlöf for skillful photographic assistance. This study has been supported by the Swedish Natural Science Research Council.

References

1. B.-O. Marinder, *Chem. Scr.* **26,** 547 (1986).
2. A. Magnéli, *Arkiv Kemi* **1,** 269 (1949).
3. F. Takusagawa and R. A. Jacobson, *J. Solid State Chem.* **18,** 163 (1976).
4. M. Lundberg, *Chem. Commun. Univ. Stockholm* **12** (1971).
5. B.-O. Marinder, *Angew. Chem.* **98,** 430 (1986).
6. A. Sleight, *Acta Chem. Scand.* **20,** 1102 (1966).
7. M. Lundberg and M. Sundberg, *J. Less-Common Met.* **137,** 163 (1988).
8. T. Hörlin, B.-O. Marinder, and M. Nygren, *Rev. Chim. Miner.* **19,** 231 (1982).
9. M. Lundberg and M. Sundberg, *Chem. Scr.* **28,** 81 (1988).
10. B.-O. Marinder and M. Sundberg, *Acta Crystallogr. Sect. C* **40,** 1303 (1984).
11. B.-O. Marinder and M. Sundberg, *Acta Crystallogr. Sect. B* **40,** 82 (1984).

12. M. O'KEEFE, P. R. BUSECK, AND S. IIJIMA, *Nature (London)* **274,** 322 (1978).
13. D. X. LI, *J. Solid State Chem.* **73,** 1 (1988).
14. S. ANDERSSON, *Acta Chem. Scand.* **19,** 2285 (1965).
15. P. APPENDINO, *Ann. Chim. (Rome)* **63,** 547 (1973).
16. A. A. AWADALLA AND B. M. GATEHOUSE, *J. Solid State Chem.* **23,** 349 (1978).
17. Ö. SÄVBORG AND M. LUNDBERG, *Mater. Res. Bull.* **15,** 1433 (1980).
18. M. LUNDBERG AND M. SUNDBERG, *J. Solid State Chem.* **63,** 216 (1986).
19. R. DE RIDDER, G. VAN TENDELOO, D. VAN DYCK, AND S. AMELINCKX, *Phys. Status Solidi A* **41,** 555 (1977).
20. S. HORIUCHI, K. MURAMATSU, AND Y. MATSUI, *J. Appl. Crystallogr.* **13,** 141 (1980).
21. S. IIJIMA AND G. ANSTIS, *in* "XXXIVth Ann. Proc. Electron Microscopy Soc. Amer." (G. W. Bailey, Ed.), p. 476, Miami Beach, FL (1976).